Magnetism in Mn_xGe_{1-x} semiconductors mediated by impurity band carriers

A. P. Li, J. F. Wendelken, and J. Shen
Condensed Matter Sciences Division and Center for Nanophase Materials Sciences, Oak Ridge National Laboratory, Oak Ridge, Tennessee 37831, USA

L. C. Feldman
Department of Physics and Astronomy, Vanderbilt University, Nashville, Tennessee 37235, USA and Condensed Matter Sciences Division, Oak Ridge National Laboratory, Oak Ridge, Tennessee 37831, USA

J. R. Thompson and H. H. Weitering
Department of Physics and Astronomy, The University of Tennessee, Knoxville, Tennessee 37996, USA and Condensed Matter Sciences Division, Oak Ridge National Laboratory, Oak Ridge, Tennessee 37831, USA
(Received 20 April 2005; revised manuscript received 22 August 2005; published 17 November 2005)

We present a comprehensive study of ferromagnetism and magnetotransport in Mn-doped germanium, grown with molecular-beam epitaxy. Ferromagnetism in Mn_xGe_{1-x} ($0<x<0.09$) is characterized by two different ordering temperatures T_C and T_C^* with $T_C \ll T_C^*$. The onset of global ferromagnetic order at T_C coincides with the percolation threshold for (activated) charge transport. Magnetism between T_C and T_C^* originates from "clustered dopants" associated with inhomogeneities. The ferromagnetic ordering temperature within the clusters is of order T_C^* while the coupling between the clusters is mediated by thermally activated carriers moving in an impurity band. The magnetoresistance exhibits nonmonotonic temperature and magnetic field dependence; both negative and positive magnetoresistance contributions are observed. The anomalous Hall effect between T_C and T_C^* appears to be influenced heavily by the large magnetoresistance. The normal and anomalous Hall coefficients both diverge at low temperature. All these observations indicate that Mn_xGe_{1-x} is most adequately described within an impurity band model where the ratio J/t of the Mn hole exchange J and hole hopping t is large.

DOI: 10.1103/PhysRevB.72.195205 PACS number(s): 75.50.Pp, 73.50.Jt, 75.70.−i

I. INTRODUCTION

Mechanisms of ferromagnetic coupling between impurity spins in dilute magnetic semiconductors (DMSs) such as $Ga_{1-x}Mn_xAs$ and $In_{1-x}Mn_xAs$ (x of order 0.05 or less) are known to be mediated by p-type charge carriers.[1–4] Ideally, each Mn dopant atom represents an acceptor that introduces a local spin and a hole carrier. Upon increasing the Mn concentration, acceptor levels above the valence band merge to form a narrow impurity band which may eventually overlap with the host valence band, depending on the doping level and binding energy of the holes. Impurity band states below the mobility edge are localized due to the randomness or disorder of the Mn lattice locations. Empirically, one finds that the hole density in DMSs is significantly smaller than the doping concentration which is due to carrier compensation or "self-compensation" by Mn interstitials[5] and/or phase separation of Mn-rich precipitates. The magnetic coupling and ordering in these materials is thus heavily affected by material issues such as carrier compensation and impurity lattice location and distribution, as well as fundamental physics issues that relate to coupling mechanisms in the presence of strong correlations and disorder. These materials indeed exhibit a very striking correlation between the transport and magnetic properties. In fact, it has been argued that DMSs exhibit interesting analogies with complex materials systems such as the colossal magnetoresistance transition-metal oxides.[6]

Studies on ferromagnetic DMSs have focused mostly on degenerately doped or "metallic" DMS materials which produce the highest ferromagnetic ordering temperature (ferromagnetic Curie temperature T_C). Insulating DMSs with lower T_C have not received as much attention, but it could be argued that the insulating regime is especially relevant for understanding the basic principles of ferromagnetism in DMSs. In this context, Mn-doped Ge appears to be especially interesting but controversial still. Following the initial report of "high-T_C" ferromagnetism in Ge (T_C=116 K; Ref. 7), several groups made great strides in their pursuit toward room-temperature ferromagnetism. Cho *et al.* have reported a ferromagnetic T_C of 285 K at 6% Mn doping level,[8] whereas Tsui *et al.* realized a T_C of 270 K by codeposition of Mn and Co.[9] These observations are especially remarkable because Mn_xGe_{1-x} DMSs are reportedly *insulating*. Recent theoretical studies employing *ab initio* full-potential linearized augmented-plane-wave supercell calculations indicated that the exchange interactions between Mn ions in Mn_xGe_{1-x} oscillate as a function of distance between them according to the Ruderman-Kittel-Kasuya-Yoshida (RKKY) formula.[10,11] Ferromagnetic ordering temperatures ranging from 134 to 400 K have even been predicted but these predictions require itinerant exchange as in metallic DMS systems.[10,11] The high-T_C reports for Mn-doped Ge therefore call for further scrutiny while the link between the nonmetallic transport properties and ferromagnetism must also be established.

In this paper, we present a comprehensive study of the ferromagnetism and electrical transport in a Mn_xGe_{1-x} DMS for Mn concentrations up to 9%. By carefully controlling the growth conditions, we obtained Mn_xGe_{1-x}, free of interme-

tallic precipitates, that exhibits not one but two magnetic phase transitions at T_C and at T_C^* with $T_C \ll T_C^*$. The magnetic response to temperature and doping concentration is indicative of global ferromagnetic ordering at $T_C = 12$ K ($x = 0.05$). T_C^* is the ferromagnetic ordering temperature within isolated spin clusters as determined from a Curie-Weiss plot of the high-temperature magnetic susceptibility; $T_C^* = 112$ K for $x = 0.05$. These spin clusters are associated with inhomogeneities in the Mn distribution. This paper expands and complements our initial report on magnetism in Mn-doped Ge,[12] with comprehensive analyses and discussions on (1) the growth procedure and (2) the spontaneous and magnetic-field-induced contributions to the magnetization and magnetotransport properties. The magnetization and anomalous Hall effect (AHE) between T_C and T_C^* are field induced, in that there is no *macroscopic* spontaneous ferromagnetic component. The AHE furthermore appears to be influenced heavily by the large magnetoresistance above T_C. The normal and anomalous Hall coefficients diverge as $T \to 0$ K, as expected for a Hall insulator and consistent with the recent theory of AHE for hopping transport.[13] The magnetoresistance appears to be dominated by fluctuation-controlled hopping between magnetic clusters. All observations consistently point toward a picture of ferromagnetic spin clusters that are exchange coupled by thermally activated charge carriers moving in an impurity band. Thus, Mn-doped Ge is distinctly different from the high-T_C III-V DMS materials.[1–3]

II. GROWTH PROCEDURES

Mn_xGe_{1-x} films were grown on undoped Ge(100) substrates with molecular-beam epitaxy (MBE). Ge substrates were cleaned *in situ* through cycles of sputtering and annealing. Before initiating the Mn flux, a thin Ge buffer layer (~150 Å) was grown at a substrate temperature of 250 °C. The Mn_xGe_{1-x} films were grown at substrate temperatures ranging from 50 to 110 °C by codeposition at a rate of 2–4 Å/mm. As will be discussed later, this low growth rate is essential for maintaining good crystalline quality at low growth temperature. The quality of the films was monitored *in situ* with reflection high-energy electron diffraction (RHEED). The persistence of a two-dimensional growth front was indicated by the streaky RHEED patterns and clear presence of (2×1) fractional order beams, originating from the well-known dimer reconstruction of the (100) surface.[14] The thickness of the films was typically 700Å, as monitored by a quartz crystal monitor *in situ* and verified *ex situ* by Rutherford backscattering spectrometry (RBS). Magnetic properties were measured using a superconducting quantum interference device (SQUID) magnetometer; electrical properties and Hall effect were measured with a four-probe configuration using a physical property measurement system (PPMS).

According to the bulk phase diagram for the Mn-Ge system,[15] there exist many intermetallic phases such as Mn_5Ge_3, $Mn_{11}Ge_8$, and Mn_2Ge. We have investigated the very delicate growth procedure for obtaining a Mn_xGe_{1-x} DMS free of known intermetallic precipitates. Figure 1 shows the temperature-dependent magnetization for samples

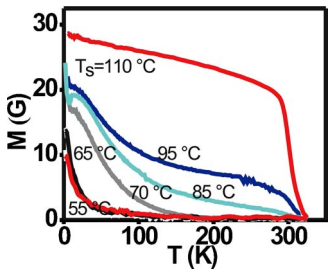

FIG. 1. (Color online) Temperature-dependent magnetic moment of $Mn_{0.05}Ge_{0.95}$ films grown at various temperatures. The applied magnetic field is 0.1 T. All magnetic quantities are per unit volume of DMS.

grown at different substrate temperatures (T_S) having the same Mn fraction $x = 0.05$. The applied magnetic field is 0.1 T. At $T_S < 50$ °C, films readily become amorphous after passing the initial growth stage. Crystalline films are obtained at $50 < T_S < 85$ °C and they are magnetic at fairly low temperature. For substrate temperatures $T_S \geq 85$ °C, and especially $T_S = 110$ °C, the films are strongly ferromagnetic with a T_C of 296±6 K. Since room-temperature ferromagnetism ($T_C \sim 296$ K) appears only at higher growth temperature, it is imperative to examine the possible formation of ferromagnetic intermetallic precipitates. It is known that Mn_5Ge_3 has a T_C of 296 K.[16] Mn_5Ge_3 is also the most stable compound in the Mn-Ge phase diagram. As shown in Fig. 1, for samples grown at $T_S \geq 85$ °C, strong ferromagnetism indicates a T_C of 296±6 K, independent of Mn concentration. This magnetic signature suggests the presence of ferromagnetic Mn_5Ge_3 alloy precipitates. Mn_5Ge_3 precipitates could not be detected with x-ray diffraction (XRD) for the (100)-oriented Mn_xGe_{1-x} thin films, however, Mn_5Ge_3 precipitates can be detected rather easily on Ge(111) with XRD and scanning tunneling microscopy as they form *epitaxially* oriented $Mn_5Ge_3(0001)$ crystallites.[17] These crystallites exhibit a magnetic signal $M(H,T)$ and T_C that is similar to that of the $Mn_xGe_{1-x}(100)$ films grown at 85 °C and above. The formation of Mn_5Ge_3 precipitates has also been observed in other Mn-doped Ge systems using transmission electron microscopy[18] and magnetic characterization.[8]

The growth rate R appears critical under these low-temperature growth conditions as well. Figure 2 compares two samples with the same Mn concentration, grown at the same $T_S = 70$ °C but with a different growth rate. At $R = 4$ Å/min, RHEED patterns (Fig. 2, inset) obtained along the [110] azimuth indicate a 2×1 reconstructed surface, with streaky fundamental and half-order diffraction features. The sample does not show a measurable magnetic response near room temperature. When the growth rate increases from 4 to 12 Å/min, the half-order RHEED streaks disappear and a three-dimensional transmission pattern is revealed, indicating a rough growth front. The deteriorating sample quality for higher growth rates leads to the appearance of the Mn_5Ge_3 signature (with $T_C \sim 296$ K) in the dc magnetization curves. This indicates that a rough growth front promotes formation of alloy precipitates. Evidently, fabrication of a Mn_xGe_{1-x} DMS ($0 < x < 9\%$) that is free of known ferromagnetic alloy precipitates requires smooth layer-by-layer

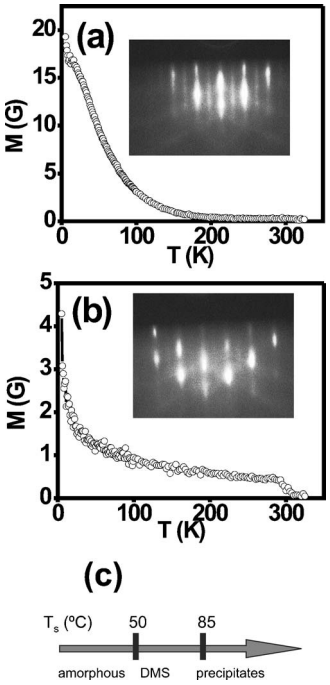

FIG. 2. Temperature-dependent magnetic moment of Mn_xGe_{1-x} films grown at different growth rates: (a) 4 and (b) 12 Å/min. The growth temperature and the nominal Mn concentration are the same in both samples: T_S=70 °C, x=5%. The applied magnetic field is 0.1 T. Insets: RHEED patterns obtained during film growth. (c) Structural phase diagram of $Mn_{0.05}Ge_{0.95}$ layers as a function of the substrate temperature grown with growth rate 4 Å/min.

growth, low growth rate, and a low growth temperature ($50<T_S<85$ °C). A one-dimensional phase diagram is sketched in Fig. 2(c) against T_S at R=4 Å/min, x=5%, and film thickness of 700 Å. We hereafter focus on the "pure" DMS phase that is free of any known intermetallic precipitates.

III. MAGNETIZATION

Figure 3(a) displays field-dependent magnetization loops for a 5.4% DMS sample free of intermetallic precipitates and grown at T_S=70 °C. The magnetic field is applied perpendicular to the film. At 5 K, the sample exhibits ferromagnetic hysteresis. Between 20 and 110 K, the magnetization loops no longer exhibit hysteresis (or remanence). The system, moreover, does not exhibit measurable magnetic anisotropy. For a concentration of 5% the saturation magnetization at 5 K is $\sim 1.0\mu_B$ per Mn atom if all Mn would contribute equally to the magnetization. Using the theoretical moment of $3\mu_B$ per Mn atom in Mn_xGe_{1-x},[7,10] we conjecture that only $\sim 1/3$ of all Mn atoms are magnetically active. Surprisingly, the moment per Mn tends to *decrease* with lower Mn concentration. Intuitively, one would have expected the opposite trend because antiferromagnetic superexchange coupling between nearest-neighbor Mn spins should be more prevalent and competing at high doping levels. Figure 3(b) compares the remanent magnetization and magnetization at 0.1 and 1 T for the x=0.054 sample. The magnetization curves are strikingly

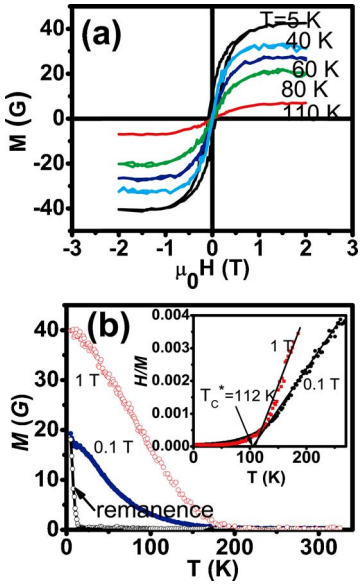

FIG. 3. (Color online) Low-temperature ferromagnetic response from Mn_xGe_{1-x} films free of alloy precipitates. (a) Field-dependent magnetization for a $Mn_{0.05}Ge_{0.95}$ thin film. (b) Remanent and field-induced magnetization of a $Mn_{0.05}Ge_{0.95}$ thin film under 0.1 and 1 T. The inset shows the Curie-Weiss extrapolation for the x=0.054 sample.

concave $[d^2M(T)/dT^2>0]$ over a broad temperature range, in contrast to the convex Brillouin-function behavior of the Stoner-Weiss mean-field theory.[19] This behavior is similar to that reported by Park *et al.*[7] but different from that of Cho *et al.*[8] In the presence of a magnetic field, the magnetization curves become less concave with measurable magnetic response extending to near 200 K. The high temperature tail of the dc "susceptibility" M/H follows a Curie-Weiss dependence as shown in the inset of Fig. 3(b). Linear fits of the H/M data for 0.1 and 1.0 T indicate an extrapolated divergence of the magnetic susceptibility at 112±5 K, in good agreement with the highest T_C=116 K reported in Ref. 7. We tentatively denote this temperature T_C^*. Magnetic remanence, however, vanishes at much lower temperature $T\sim 12$ K. It is noted that in the presence of a 0.1 T magnetic field, the temperature-dependent magnetization curve also displays a small cusp near 12 K.

Magnetic ac susceptibility measurements as a function of temperature indicated that the irreversible magnetization sets in at a much lower temperature T_C.[12] The onset of global ferromagnetism occurs at T_C and not at T_C^*. The location of T_C determined from the cusp in the susceptibility coincides with the disappearing remanence for all $x<0.009$. T_C increases almost linearly with x up to ~ 0.09, whereas T_C^* saturates at $x>0.05$ as reported previously.[12] Still higher doping concentration ($x>0.09$) resulted in rough growth fronts and inclusion of intermetallic precipitates so the resulting magnetic response is not considered characteristic of a Mn_xGe_{1-x} DMS.

Since Mn_xGe_{1-x} DMSs do not exhibit magnetic remanence between T_C and T_C^*, it is imperative to examine whether T_C represents a superparamagnetic blocking transition instead of a ferromagnetic transition temperature. The

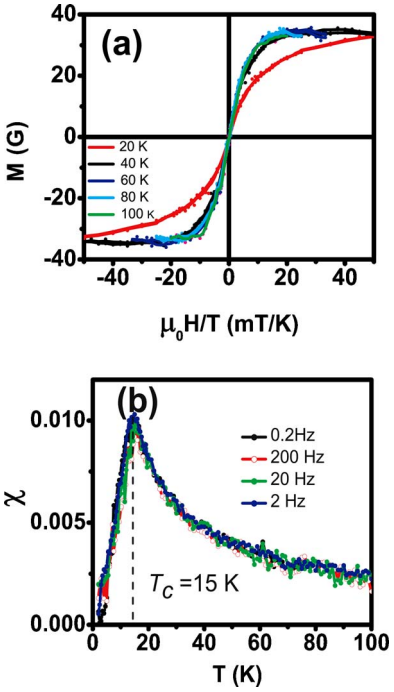

FIG. 4. (Color online) (a) The magnetization curves at different temperatures presented as a Langevin plot. (b) Temperature-dependent ac susceptibility of $Mn_{0.07}Ge_{0.93}$ films measured with different ac frequencies f. H_{dc}=0 Oe, H_{ac}=5 Oe.

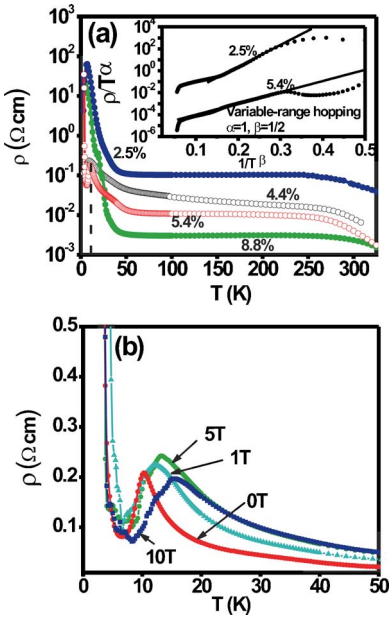

FIG. 5. (Color online) (a) Temperature-dependent resistivity of Mn_xGe_{1-x} films in zero magnetic field for various Mn content. Inset: Analyzed resistivity of two films as function of inverse temperature, revealing variable-range-hopping conduction. (b) Resistivity of a $Mn_{0.05}Ge_{0.95}$ film in various magnetic fields, showing progressive shift of the peak.

magnetization of a superparamagnet follows a Langevin function when plotting M/M_s versus H/T.[19] As shown in Fig. 4(a), high-temperature magnetization data collapse onto the Langevin function ($T>40$ K) but the 20 K data clearly deviate from the superparamagnetic response. Notice that T_C is even lower: 12 K. Frequency-dependent measurements also rule out traditional superparamagnetic blocking behavior. According to the Neel-Brown theory of superparamagnetism,[20] the blocking temperature T_B of *non-interacting* spin clusters is given by

$$T_B \sim \Delta E/\mathrm{In}(\tau/\tau_0)k_B, \tag{1}$$

with ΔE being the energy barrier to magnetization reversal in a single spin cluster, τ the measurement time, proportional to $1/f$, τ_0 the attempt time, and k_B the Boltzmann constant. The superparamagnetic blocking temperature depends on the measurement frequency f. The magnitude of the factor $\Delta T_B/T_B\Delta(\mathrm{In}f)$ is typically of order 0.1 in superparamagnets.[19] However, as shown in Fig. 4(b), frequency-dependent measurements did not reveal any measurable shift of T_C over three decades of frequency within the resolution of the experiment (0.2 K). This is indicative of true ferromagnetism as opposed to superparamagnetism or due to the presence of strongly interacting magnetic dipoles.[19] At any rate, the magnetic transition at T_C is not a conventional superparamagnetic blocking transition. A spin-glass transition is also highly unlikely because the magnetization of a spin glass would be extremely hard to saturate[21] while a Mn_xGe_{1-x} DMS saturates at 1–2 T. It is thus concluded that T_C corresponds to a ferromagnetic ordering temperature. T_C^*, on the other hand, represents an extrapolated Curie-Weiss transition temperature. The large separation between T_C and T_C^* suggests the presence of carrier-mediated interacting spin clusters, as discussed in Sec. V.

IV. TRANSPORT PROPERTIES

A. Magnetoresistance

Figure 5(a) shows the zero-field resistivity as a function of temperature for films with different Mn concentrations. Electrical transport reveals insulating behavior over the entire temperature range with the apparent exception of a cusp near T_C. For all samples with $x<8.8\%$, the resistivity shows a clear peak exactly at T_C and diverges as $T\rightarrow 0$ K. For the 8.8% sample, resistivity does not drop as dramatically below T_C, but rather exhibits a shoulder. This is very surprising because heavily doped III-V semiconductors are metallic. These features near T_C in the resistivity do not indicate a metal-insulator transition as reported in $Ga_{1-x}Mn_xAs$ DMSs,[1,22] because the conduction remains activated as the temperature approaches zero K. The decrease of resistivity above 200 K is dominated by parallel conductance through the substrate.

The insulating behavior of Mn_xGe_{1-x} DMSs indicates that the Fermi level is located below the mobility edge of the Mn-induced impurity band. In such a localized system, phonon-assisted hopping becomes the dominant mechanism for charge transport at low temperatures. The variable-range hopping formula for doped semiconductors at low temperature is[23]

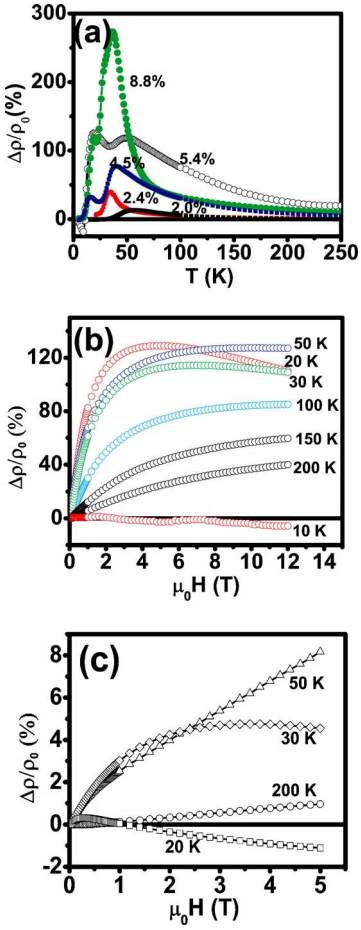

FIG. 6. (Color online) Magnetoresistance of Mn_xGe_{1-x} films. (a) Temperature-dependent magnetoresistance for samples with different Mn content at 5 T magnetic field. (b) Field-dependent magnetoresistance of a $Mn_{0.05}Ge_{0.95}$ film at various temperatures. (c) Field-dependent magnetoresistance of a $Mn_{0.02}Ge_{0.98}$ film at various temperatures

$$\rho(T) \propto T^{\alpha}\exp[(T_0/T)^{\beta}] \tag{2}$$

where the hopping exponent β equals $\frac{1}{4}$ for Mott variable-range hopping and $\frac{1}{2}$ for Efros-Shklovskii (ES) hopping. The ES formula accounts for electron-electron interactions and the presence of a soft Coulomb gap at the Fermi level; α is a nonuniversal power-law exponent while k_BT_0 represents the average energy level spacing within the localization length. The optimal fit to our low-temperature data suggests ES hopping, i.e., $\alpha=1$ and $\beta=1/2$ in approximately 1–2 decades of resistivity; see inset of Fig. 5(a).

The presence of a magnetic field has a profound influence on the transport behavior of Mn_xGe_{1-x} DMSs. The resistivity cusp shifts to higher temperature in the presence of a magnetic field as shown in Fig. 5(b) for the 5.4% sample. The magnetoresistance (MR) is defined as

$$\Delta\rho/\rho_0 = [\rho(H) - \rho(0)]/\rho(0) \tag{3}$$

where $\rho(0)$ and $\rho(H)$ are the resistivities in the absence or presence of a magnetic field H, respectively. Figure 6(a) shows the MR as a function of temperature for samples with different Mn concentration in the presence of a 5 T magnetic field. A very large positive MR is observed above T_C. At a temperature between T_C and T_C^*, the MR experiences a peak (a second peak appears in 5.4% and 4.5% samples) and then decreases with increasing temperature. The maximum MR value increases with the Mn concentration x. The field-dependent MR at various temperatures is shown in Figs. 6(b) and 6(c), respectively, for 5.4% and 2.0% samples. Below T_C, the sign and slope of the field-dependent MR are both negative. At intermediate temperatures (e.g., 20 and 30 K), the MR contains two contributions: a positive onset is followed by a negative slope at higher field, thus producing a maximum in the MR. At high temperatures (e.g., 50–300 K), we only observe a large positive MR. Qualitatively similar behavior has been reported for GaAs/MnAs (Refs. 24–26) and Mn_5Ge_3/Ge (Ref. 18) nanoscale hybrid structures. Thus, nonmonotonic behavior of the magnetoresistance seems to be a hallmark of hybrid systems containing ferromagnetic nanoclusters (see Sec. V).

B. Anomalous Hall effect

The Hall effect of Mn_xGe_{1-x} DMSs is dominated by an anomalous Hall effect. The Hall resistivities ρ_{Hall} were measured as a function of temperature and magnetic field. For a *metallic* ferromagnet at fixed temperature, the Hall resistivity follows $\rho_{Hall}=R_0B+\mu_0R_sM$ where B is the magnetic induction in the interior of the sample, and R_0 and R_s are the normal and anomalous Hall coefficients, respectively. This empirical relation is also indicated by recent studies of the AHE in Mn:GaAs DMSs.[23] As will be shown, a similar relation is established for Mn_xGe_{1-x} DMSs. The precise physical meaning of the "constants" R_0 and R_s for nonmetallic DMSs remains to be determined, however.

For a uniformly magnetized body, the effective magnetizing field (vector) is $H_{eff}=H_a-N\cdot M$, where H_a is the applied field and the tensor N contains various demagnetization factors. For a thin film with magnetic field applied perpendicular to its plane, the magnetic induction $B=\mu_0H_a+\mu_0(1-N_\perp)M$ and with $N_\perp\approx1$ and $M\ll H_a$, the Hall resistivity becomes

$$\rho_{Hall}(H) = R_0(H)\mu_0H + R_s(H)\mu_0M \tag{4}$$

where for simplicity we now write $H_a=H$. The first term on the right-hand side of Eq. (4) represents the normal Hall effect while the second term is the AHE. For DMS materials, the Hall "constants" $R_0(H)$ and $R_s(H)$ could be field dependent. The field-dependent Hall resistivities measured at various temperatures are shown in Fig. 7. The Hall resistivity increases rapidly below T_C^*, which is due to the overwhelming contribution from the AHE, consistent with the empirical relation Eq. (4).

The spontaneous Hall coefficient of *metallic* ferromagnets usually follows $R_s=\alpha'\rho+\beta'\rho^2$ where ρ is the longitudinal resistivity; α' and β' are constants. Theories have attributed the AHE to impurity scattering in the presence of spin-orbit interaction. Traditionally, the linear term has been attributed to "skew scattering" while the quadratic term represents the "side jump." Although the physics of the AHE is different for

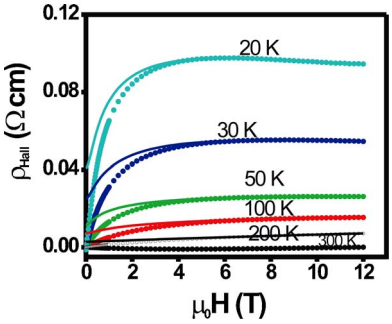

FIG. 7. (Color online) Field-dependent Hall resistivity of a $Mn_{0.05}Ge_{0.95}$ film at various temperatures. Solid dots, experimental data; solid lines, fitting curves to Eq. (4).

Hall insulators, we can establish an *empirical* relation between $R_s(H)$ and $\rho(H)$. To first order, we ignore the normal Hall effect contribution and plot $\rho_{Hall}(H)/\mu_0 M(H) \approx R_S(H)$ versus $\rho(H)$ as shown in Fig. 8 for the 5.4% sample. This plot compiles the information from the magnetization isotherms and from the Hall-effect and magnetoresistance isotherms (notice that these curves do not go through the origin). Clearly, $R_s(H)$ of nonmetallic Mn_xGe_{1-x}, is linear in $\rho(H)$ for each isotherm in Fig. 8. This is true for nearly all temperatures and for all values of $x<0.009$ although α' is temperature dependent, especially close to T_C^*.

Notice that the Hall resistivity varies linearly with H above ~5 T (Fig. 7), which greatly facilitates the extraction of the normal Hall coefficient. R_0 is usually determined from $\partial\rho_{Hall}/\partial H$ at high magnetic field where the magnetization and AHE contribution are saturated. However, because the magnetoresistance is large, the high-field slope of the Hall isotherms will be influenced by magnetoresistance through the empirically established correlation between $R_s(H)$ and $\rho(H)$. In fact, the constant $(\partial\rho_{Hall}/\partial H)_T$ at high magnetic fields implies that up to first order in H, $R_0(H)=R_0$ is a constant while $R_s(H)$ is linear in H; higher-order dependencies are negligible at high field. Accordingly, R_0 is determined from

$$\left(\frac{\partial\rho_{Hall}}{\partial H}\right)_T \cong \mu_0 R_0 + \alpha'\mu_0\left(\frac{\partial\rho}{\partial H}\right)_T M_T, \qquad (5)$$

where M_T is the saturation magnetization at temperature T. $R_s(H=0)$ is determined by extrapolating $\rho_{Hall}(H)$ to zero

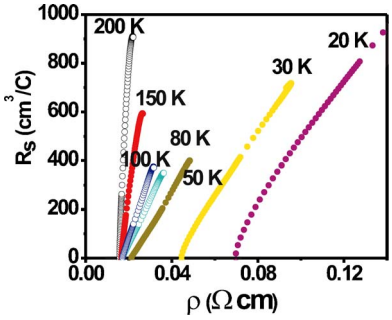

FIG. 8. (Color online) Anomalous Hall coefficients $R_s(H)$ demonstrating a linear dependence on $\rho(H)$ at various temperatures.

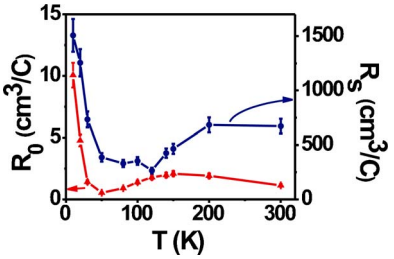

FIG. 9. (Color online) Normal (R_0) and anomalous (R_s) Hall coefficients versus temperature.

field. To check the validity of this procedure, we fitted the $\rho_{Hall}(H)$ isotherms to the experimental values of $M(H)$, $\rho(H)$, and R_0, using α' as a free parameter. The fitted results are displayed in Fig. 7 as solid curves, together with the experimental Hall data. The fits are quite good at high fields but as expected, the fits deviate from the experimental data at low fields where the magnetization and transport properties display more complicated field dependence. R_0 indicates p-type conduction for all T. Notice that the experimental high-field slopes in the raw data change from negative to positive as the temperature increases. If we had ignored the magnetoresistance contribution to $R_s(H)$, we would have attributed the change of slope to a sign change of the normal Hall coefficient, R_0.

The normal and anomalous Hall coefficients are shown in Fig. 9. In contrast to the case of band transport through extended states, the normal Hall effect does not relate to a carrier density in the case of hopping conduction. Instead, it derives from the interference of different hopping trajectories.[13,27] For hopping conduction, the *leading* temperature dependence of R_0 and $R_s(H=0)$ should follow $\exp(T_0/T)^{1/2}$, i.e, both quantities diverge as $T\to 0$ K.[13,23] This is qualitatively consistent with our observations in Fig. 9. Both $\rho\propto\exp(T_0/T)^{1/2}$ and R_0 change by about one decade between T_C and 50 K while $R_s(H=0)$ changes by about a factor of 4. $R_s(H)$ is furthermore proportional to the derivative of the density of states near the Fermi level, which is located in the impurity band.[13] The poor fitting of ρ_{Hall} at low fields (Fig. 7) could thus be related in part to magnetic-field-induced changes in the density of states and, consequently, to the changes in $R_s(H)$.[28]

The spontaneous magnetization of conventional ferromagnets should disappear above T_C. For Mn-doped Ge DMSs, however, the AHE remains visible above T_C due to the strong field-induced magnetization [Fig. 3(b)]. Strictly speaking, the AHE above T_C does *not* represent a spontaneous Hall effect but a field-induced phenomenon. T_C^* appears to be the relevant ordering temperature here. In fact, T_C^* can be determined from the Hall isotherms by converting them into an Arrott plot.[19] Conventionally, the Arrott construction is a plot of M^2 versus H/M that is used to determine the ferromagnetic ordering temperature from $M(H)$ data measured at different temperatures. Because the AHE term is the dominant term up to room temperature as shown in Figs. 7 and 9, M scales approximately with (ρ_{Hall}/ρ). Following the procedure of Ohno,[29] we have plotted $(\rho_{Hall}/\rho)^2$ versus $H/(\rho_{Hall}/\rho)$ for each temperature (Fig. 10). The high-field

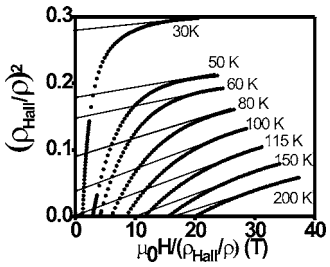

FIG. 10. Arrott plot of $Mn_{0.05}Ge_{0.95}$ from the longitudinal and Hall resistivities at different temperatures and magnetic fields; see text.

isotherm extending through the origin yields the ferromagnetic transition temperature, which is 115 K for the 5.4% sample. This ferromagnetic transition temperature coincides within experimental uncertainty with the extrapolated Curie-Weiss value T_C^* of 112 K, confirming the result and validity of the earlier Curie-Weiss extrapolation [Fig. 3(b) inset].

V. DISCUSSION

In order to discuss the magnetic and transport phenomena, we first summarize the observations. (1) The Mn-doped Ge DMS is not a high-T_C semiconductor. The ferromagnetic transition near room temperature[8] originates from known intermetallic phases such as Mn_5Ge_3, whereas the $T_C=116$ K reported in Ref. 7 must be interpreted as a T_C^*. (2) There exist two ferromagnetic transitions T_C and T_C^* ($T_C \ll T_C^*$) which depend linearly on the doping concentration, followed by saturation for $x>0.054$ in the case of T_C^*. The magnetic response between T_C and T_C^* deviates from conventional superparamagnetism as T approaches T_C from above. (3) Strong correlation occurs between magnetism and transport near both transitions: T_C coincides with a resistivity cusp and sign reversal of the magnetoresistance while the Curie-Weiss extrapolation and anomalous Hall effect consistently point toward the existence of a T_C^*. (4) Transport is thermally activated as is evident from the temperature dependence of ρ, R_0, and R_s above T_C. (5) $M(T)$ is strikingly concave. Finally (6) the magneto-resistance is very large and exhibits a nonmonotonic field dependence above T_C.

Considering first the activated transport (observation 4), RKKY-type exchange via itinerant valence band holes can be ruled out as the dominant mechanism of ferromagnetism in Mn_xGe_{1-x}. By definition, the RKKY picture can only hold for itinerant carriers. The samples are insulating over the entire temperature range (i.e., $d\rho/dT<0$, except near the cusp at T_C) and the onset temperature for global ferromagnetism (T_C) is only of the order of 10 K, much lower than for the itinerant III-V DMS materials. Our observations point toward a picture of localized carriers moving in a narrow impurity band. Notice that the hole binding energy is $\sim$160 meV above the valence band maximum,[30] and therefore impurity band physics must be operational in the strongly localized regime and carriers are strongly bound to the randomly located magnetic impurities. Thus Mn_xGe_{1-x} is most adequately described within an impurity band model where the ratio J/t of the Mn hole exchange J and hole hopping integral t is large (strong-coupling limit[6,31]).

The magnetic observations 2 and 5 are consistent with long-range ferromagnetic FM order below T_C and short range order between T_C and T_C^*. Clearly, the magnetization below T_C is spontaneous while the magnetization and AHE above T_C are field induced. The concavity of $M(T)$ is also typical for localized systems.[32] To determine whether the concavity is due to departures from weak-coupling behavior or whether convex behavior can be restored via postannealing,[1,33,34] we measured the remanence after post annealing to 100 and 200 °C. Interestingly, both T_C and T_C^* increased but the remanent magnetization became even more concave demonstrating that the concave behavior is a fundamental feature of ferromagnetism in the Mn_xGe_{1-x} DMS that clearly differs from the ferromagnetism of high-T_C $Ga_{1-x}Mn_xAs$.[33,34] None of the postannealed samples exhibited signatures of intermetallic precipitates.[35]

The strong correlation between the transport and magnetic data indicates that the ferromagnetic interaction is mediated by thermally activated carriers moving in an impurity band. Perhaps the strongest indication of activated-carrier-mediated exchange is the observed agreement between magnetization data and the magnetization inferred from AHE data; particularly the consistency between the T_C^* from the Curie-Weiss extrapolation and the Arrott analysis of the AHE.

Ferromagnetism within an impurity band suggests that ferromagnetic coupling is mediated by "double exchange,"[36] not a RKKY coupling. The double-exchange mechanism will only be operative if the Mn holes are partially compensated (allowing single-hole occupancy only on the localization sites).[5] Recently, Kaminski and Das Sarma (KDS) developed a percolation theory for strongly compensated DMS materials which assumes that $n_i \gg n_h$ as is usually the case with DMSs.[32,37] The exchange interaction between the localized charge carrier and surrounding Mn ions leads to the formation of a bound magnetic polaron. Within the KDS formalism, T_C^* would correspond to the temperature where a localized hole carrier and neighboring Mn spin form the seed of a "bound magnetic polaron," i.e., T_C^* would equal the Mn hole exchange coupling J.[38] Alternatively, if the dopant distribution were inhomogeneous, T_C^* would be the effective ferromagnetic transition temperature for a "typical" cluster containing several holes. As the temperature drops below T_C^*, these polaronic clusters grow in size and eventually percolate to form an infinite ferromagnetic cluster at $T_C=12$ K ($x=0.05$). This ferromagnetic percolation would establish a transport path with a strongly diminished exchange contribution to the hopping barriers.[37] For strongly localized carriers and low doping concentrations, the size of the bound magnetic polaron grows logarithmically slowly as the temperature decreases.[37] The resistivity will very much depend on the actual percolation scenario and hopping trajectories of the hole which would probably be sample dependent, but it is expected to increase monotonically upon cooling as the vanishing exchange barrier is offset by the decreased hopping probability at lower temperature.[39] Alternatively, at higher doping levels, ferromagnetic percolation and transport percolation do coincide if dopants are grouped into clusters, lead-

ing to an abrupt reduction of the transport activation barrier (or vanishing exchange barrier) just below T_C. This scenario is perfectly consistent with the observed dip in the resistivity below T_C. The field-induced shift of the resistivity maximum [Fig. 6(b)] further corroborates the close connection between magnetic and transport percolation, as in other doped polaronic systems where inhomogeneities play an important role.[40] The fact that T_C^* saturates at $x=0.054$ whereas T_C increases all the way up to $x=0.09$ suggests that the saturation of T_C^* is not related to a competition between carrier-mediated ferromagnetic exchange and antiferromagnetic Mn-Mn superexchange. Rather, we speculate that the saturation of T_C^* is due to a finite size effect, i.e, when $x>0.054$, the average cluster size increases beyond the ferromagnetic interaction radius at that temperature.

At this point, we need to be more explicit about the nature of the imhomogeneities or meaning of the word "cluster." So far, we have been able to rule out clusters of known intermetallic phases. However, the sharp dip in the resistivity as well as the existence of a T_C^* suggests that dopants may be grouped into clusters. The absence of superparamagnetic H/T scaling and the field-dependent magnetotransport (see below) also point toward interacting clusters. Moreover, the existence of Mn clusters in Ge was observed previously by transmission electron microscopy[7] and by scanning photoelectron microscopy;[41] however, these clusters do not correspond to any known bulk phase precipitates.[7,41] Mn clustering is not due to a random fluctuation of the Mn dopants. In fact, it has been argued theoretically that Mn impurities should group in clusters in GaAs (Refs. 42 and 43) and in II-VI systems,[44] due to electrostatic interactions during MBE growth. We conjecture that such a physical cluster can be viewed as a generalization of the bound magnetic polaron, one that contains many Mn atoms and possibly several holes. The characteristic size of the wave function will likely be of the order of the cluster size so that ferromagnetic exchange within the cluster can overcome the competing Mn-Mn antiferromagnetic superexchange. The ordering temperature with the clusters is of order T_C^*. The clusters become coupled at T_C. Clustered states have also been proposed by Alvarez and Dagotto.[6,45] In fact, the large separation between T_C and T_C^* would place Mn_xGe_{1-x} DMSs in the strong-coupling regime ($J \gg t$) of the magnetic phase diagram of a single-band DMS.[45]

We finally address the field-dependent magnetotransport data (Fig. 6). In polaronic systems, one would expect the MR to be negative as the magnetic field aligns the polarons and thereby reduces the exchange barrier for activated hopping. This interpretation is consistent with our data below T_C. However, the MR above T_C is far more complicated. The MR increases rapidly at low fields and then decreases almost linearly at higher fields. Positive MR is usually attributed to the Efros-Shklovskii mechanism: the magnetic field shrinks the wave function and thereby effectively reduces the radius in the hopping probability. A second mechanism for clustered inhomogeneities or embedded ferromagnetic nanoclusters in a semiconductor matrix was proposed recently by Schmidt *et al.*[46] This mechanism emphasizes fluctuations in the magnitude and orientation of the magnetization of the nanoclusters. A magnetic field suppresses these fluctuations and thereby reduces the probability that a trapped hole hops from one magnetic polaron site to another. Meanwhile, the magnetic field also reduces the polaron barrier, hence there are two competing effects: the MR is positive for relatively small magnetic fields and negative for larger magnetic fields, in qualitative agreement with the present observations. Recently, Michel *et al.* have theoretically analyzed the interplay of disorder effects and magnetic-field-induced band filling effects and its influence on the MR of DMSs.[28] Both positive and negative MR effects have been predicted by weighting disorder and occupation effects as a function of temperature and magnetic field. All these mechanisms imply that the clusters are coupled magnetically via thermally activated holes.

VI. CONCLUSION

In conclusion, ferromagnetism in Mn_xGe_{1-x} is consistent with impurity band physics and an inhomogeneous distribution of Mn dopants. There is no evidence of RKKY-type ferromagnetism,[10,11] nor is there any evidence of T_C approaching room temperature.[8] The anomalous Hall effect indicates a ferromagnetic Hall insulator and suggests that the ferromagnetic coupling up to T_C^* is mediated by thermally activated carriers moving in an impurity band. The two magnetic transitions and concavity of $M(T)$ are clearly more compatible with cluster models than with a weak-coupling J picture where the carriers are homogeneously distributed. Specifically, the ferromagnetic and transport percolation at T_C and presence of spin clusters between T_C and T_C^* suggest that the physics of Mn_xGe_{1-x} DMSs is somewhat similar to that of other doped magnetic systems, including colossal magneto resistance materials.[6,47] Detailed theoretical studies are called for, including the magnetotransport properties and compositional dependence of T_C and T_C^*, to fully confirm this picture.

ACKNOWLEDGMENTS

The authors greatly appreciate stimulating discussions with Andrei Pethukov, Sankar Das Sarma, Elbio Dagotto, and S. T. B. Goennenwein, and thank Y. Song for the RBS calibration measurements. This work was sponsored by the NSF under Contract No. DMR-0306239 (F.R.G.) and by the LDRD Program of Oak Ridge National Laboratory, managed by UT-Battelle, LLC, for the U.S. Department of Energy under Contract No. DE-AC05-00OR22725.

[1] A. H. MacDonald, P. Schiffer, and N. Samarth, Nat. Mater. **4**, 195 (2005).
[2] C. Timm, J. Phys.: Condens. Matter **15**, R1865 (2003).
[3] T. Dietl, H. Ohno, F. Matsukura, J. Cibert, and D. Ferrand, Science **287**, 1019 (2000).
[4] D. J. Keavney, D. Wu, J. W. Freeland, E. Johnston-Halperin, D. D. Awschalom, and J. Shi, Phys. Rev. Lett. **91**, 187203 (2003).
[5] S. C. Erwin and A. G. Petukhov, Phys. Rev. Lett. **89**, 227201 (2002).
[6] G. Alvarez, M. Mayr, and E. Dagotto, Phys. Rev. Lett. **89**, 277202 (2002).
[7] Y. D. Park, A. T. Hanbicki, S. C. Erwin, C. S. Hellberg, J. M. Sullivan, J. E. Mattson, T. F. Ambrose, A. Wilson, G. Spanos, and B. T. Jonker, Science **295**, 651 (2002).
[8] S. Cho, S. Choi, S. C. Hong, Y. Kim, J. B. Ketterson, B.-J. Kim, Y. C. Kim, and J.-H. Jung, Phys. Rev. B **66**, 033303 (2002).
[9] F. Tsui, L. He, L. Ma, A. Tkachuk, Y. S. Chu, K. Nakajima, and T. Chikyow, Phys. Rev. Lett. **91**, 177203 (2003).
[10] A. Stroppa, S. Picozzi, A. Continenza, and A. J. Freeman, Phys. Rev. B **68**, 155203 (2003).
[11] Y.-J. Zhao, T. Shishidou, and A. J. Freeman, Phys. Rev. Lett. **90**, 047204 (2003).
[12] A. P. Li, J. Shen, J. R. Thompson, and H. H. Weitering, Appl. Phys. Lett. **86**, 152507 (2005).
[13] A. A. Burkov and L. Balents, Phys. Rev. Lett. **91**, 057202 (2003).
[14] R. D. Aburano, H. Hong, K.-S. Chung, M. C. Nelson, P. Zschack, H. Chen, and T.-C. Chiang, Phys. Rev. B **57**, 6636 (1998).
[15] E. Wachtel and E.-T. Henig, Z. Metallkd. **60**, 243 (1969).
[16] N. Yamada, J. Phys. Soc. Jpn. **59**, 273 (1990). A competing germanide compound with slightly lower Mn content is $Mn_{11}Ge_8$. It has a T_C of 274 K.
[17] C. Zeng, S. C. Erwin, L. C. Feldman, A. P. Li, R. Jin, Y. Song, J. R. Thompson, and H. H. Weitering, Appl. Phys. Lett. **83**, 5002 (2003).
[18] Y. D. Park, A. Wilson, A. T. Hanbicki, J. E. Mattson, T. Ambrose, G. Spanos, and B. T. Jonker, Appl. Phys. Lett. **78**, 2739 (2001).
[19] S. I. S. Jacobs and C. P. Bean, in *Magnetism*, edited by G. T. Rado and H. Suhl (Academic, New York, 1963), Vol. 3.
[20] W. F. Brown, Phys. Rev. **130**, 1677 (1963).
[21] J. A. Mydosh, *Spin Glasses: An Experimental Introduction* (Taylor and Francis, London, 1993).
[22] A. Van Esch, L. Van Bockstal, J. De Boeck, G. Verbanck, A. S. van Steenbergen, P. J. Wellmann, B. Grietens, R. Bogaerts, F. Herlach, and G. Borghs, Phys. Rev. B **56**, 13103 (1997).
[23] W. Allen, E. G. Gwinn, T. C. Kreutz, and A. C. Gossard, Phys. Rev. B **70**, 125320 (2004).
[24] S. Ye, P. J. Klar, Th. Hartmann, W. Heimbrodt, M. Lampalzer, S. Nau, T. Torunski, W. Stolz, T. Kurz, H.-A. Krug von Nidda, and A. Loidl, Appl. Phys. Lett. **83**, 3927 (2003).
[25] P. J. Wellmann, J. M. Garcia, J. L. Feng, and P. M. Petroff, Appl. Phys. Lett. **73**, 3291 (1998).
[26] H. Akinaga, J. De Boeck, G. Borghs, S. Miyanishi, A. Asamitsu, W. Van Roy, Y. Tomioka, and L. H. Kuo, Appl. Phys. Lett. **72**, 3368 (1998).
[27] Y. M. Gal'perin, E. P. German, and V. G. Karpov, Sov. Phys. JETP **72**, 193 (1991).
[28] C. Miche, P. J. Klar, S. D. Baranovskii, and P. Thomas, Phys. Rev. B **69**, 165211 (2004).
[29] H. Ohno, Science **281**, 951 (1998).
[30] H. H. Woodbury and W. W. Tyler, Phys. Rev. **100**, 659 (1955).
[31] G. Alvarez and E. Dagotto, Phys. Rev. B **68**, 045202 (2003).
[32] A. Kaminski and S. Das Sarma, Phys. Rev. Lett. **88**, 247202 (2002).
[33] S. J. Potashnik, K. C. Ku, S. H. Chun, J. J. Berry, N. Samarth, and P. Schiffer, Appl. Phys. Lett. **79**, 1495 (2001).
[34] K. W. Edmonds, P. Boguslawski, K. Y. Wang, R. P. Campion, S. N. Novikov, N. R. S. Farley, B. L. Gallagher, C. T. Foxon, M. Sawicki, T. Dietl, M. B. Nardelli, and J. Bernholc, Phys. Rev. Lett. **92**, 037201 (2004).
[35] A. P. Li, J. Shen, and H. H. Weitering (unpublished).
[36] C. Zener, Phys. Rev. **82**, 403 (1951).
[37] S. Das Sarma, E. H. Hwang, and A. Kaminski, Phys. Rev. B **67**, 155201 (2003).
[38] S. Das Sarma (private communication).
[39] A. Kaminski and S. Das Sarma, Phys. Rev. B **68**, 235210 (2003).
[40] M. Jaime, H. T. Hardner, M. B. Salamon, M. Rubinstein, P. Dorsey, and D. Emin, Phys. Rev. Lett. **78**, 951 (1997).
[41] J.-S. Kang, G. Kim, S. C. Wi, S. S. Lee, S. Choi, Sunglae Cho, S. W. Han, K. H. Kim, H. J. Song, H. J. Shin, A. Sekiyama, S. Kasai, S. Suga, and B. I. Min, Phys. Rev. Lett. **94**, 147202 (2005).
[42] Ph. Ebert, T. Zhang, F. Kluge, M. Simon, Z. Zhang, and K. Urban, Phys. Rev. Lett. **83**, 757 (1999).
[43] C. Timm, F. Schafer, and F. von Oppen, Phys. Rev. Lett. **89**, 137201 (2002).
[44] H. Bednarski, J. Cisowski, and J. C. Portal, Phys. Rev. B **55**, 15762 (1997); S. J. Weston, M. O'Neill, J. E. Nicholls, J. Miao, W. E. Hagston, and T. Stirner, *ibid.* **58**, 7040 (1998); P. Harrison, J. M. Fatah, T. Stirner, and W. E. Hagston, J. Appl. Phys. **79**, 1684 (1996)).
[45] M. Mayr, G. Alvarez, and E. Dagotto, Phys. Rev. B **65**, 241202(R) (2002).
[46] D. R. Schmidt, A. G. Petukhov, M. Foygel, J. P. Ibbetson, and S. J. Allen, Phys. Rev. Lett. **82**, 823 (1999).
[47] J. M. De Teresa, M. R. Ibarra, P. A. Algarabel, C. Ritter, C. Marquina, J. Blasco, J. García, A. del Moral, and Z. Arnold, Nature (London) **386**, 256 (1997).